# ACOUSTIC EMISSION MONITORING OF STEEL-FIBER REINFORCED CONCRETE BEAMS UNDER BENDING

**DIMITRIOS G. AGGELIS [1], DIMITRA SOULIOTI [1], NEKTARIA M. BARKOULA [1], ALKIVIADIS S. PAIPETIS [1], THEODORE E. MATIKAS [1] and TOMOKI SHIOTANI [2]**

[1] Dept. of Materials Science and Engineering, University of Ioannina, Ioannina 45110, Greece;
[2] Dept. of Urban Management, Graduate School of Engineering, Kyoto University, C1-2-236, Kyoto-Daigaku-Katsura, Nishikyo, Kyoto 615-8540, Japan

## Abstract

The present paper describes acoustic emission (AE) behavior of concrete under four-point bending. Different contents of steel fiber were included to investigate their influence on the load-bearing capacity, as well as on the fracture mechanisms. The main crack was accompanied by many minor cracks indicating that the fibers increased the width of the fracture process zone. The total AE activity was directly proportional to the fiber content. The subsequent study of the AE waveform characteristics revealed that the increase in the fiber content resulted in a shift from the tensile to the shear mode of failure due to improvement of the weak tensile properties of concrete.

**Keywords**: Bending, concrete, fracture mode, steel fibers.

## Introduction

The application of fiber reinforcement in cementitious materials continues to expand. Fibers restrain the breakage of the brittle matrix and enhance its weak tensile properties (Stahli and van Mier, 2007). As the content of the fibers increases, the possibility that the crack growth will be hindered through an arrest mechanism also increases. As a result, the material toughness is also increased (Mobasher et al., 1990, Sivakuram and Sathanam, 2007). An unreinforced concrete member fails catastrophically at the maximum load. Fibers mainly improve its post-peak behavior, while in many cases the maximum load is also significantly increased (Fischer and Li, 2007, Washer et al. 2004).

To clarify the mechanisms for this behavior, acoustic emission (AE) monitoring has been carried out during fracture tests. There are numerous applications of the AE technique for damage characterization of concrete structures (Shiotani and Aggelis, 2007, Shiotani et al. 2007, 2001, Aggelis et al. 2007, Triantafyllou and Papanikolaou, 2006, Golaski et al., 2006, Shah and Weiss 2006). Study of the AE behavior can lead to the characterization and quantification of the damage level via the use of AE descriptors and thus provides an early warning prior to the macroscopically observed fracture. Further study of the transient waveforms provides information about the fracture process. The source of the AE activity is closely connected to the mode of fracture (Shigeishi and Ohtsu, 1999). Nucleation of shear cracks follows tensile crack nucleation. Therefore, the determination of the dominant mode provides an early warning prior catastrophic failure. However, the application of AE to such materials entails certain difficulties. These mainly concern the accurate interpretation of the results due to the different individual processes that contribute to the fracture of concrete. Fracture occurs between different interfaces; cement paste and sand, mortar and aggregates, concrete and fibers. Additionally, failure includes aggregate crushing and fiber rupture (Kumar and Gupta, 1996). The fracture process of fiber reinforced concrete can be divided in three distinct stages. The first is the "micro-cracking stage".

The second stage is the growth of micro-cracks and development of macro-cracks up to a saturation level. The final stage includes the rapid expansion of the macro-cracks and the material's macroscopic fracture (Wu et al. 2000, 2001, Kim and Weiss, 2003, Weiler et al. 1996).

In the present study, steel-fiber reinforced concrete beams were subjected to four-point bending with simultaneous recording of their AE behavior. An increase of the maximum load and toughness with fiber content was observed, as expected. The improvement of the weak tensile behavior of concrete with the addition of fibers was mirrored in the recorded AE activity, which exhibited events with more "shear" character. Finally, the number of hits correlated well with the measured toughness properties of the reinforced concrete.

**Experimental Part**

The specimens were square beams with dimensions 100x100x400 mm. The mix was typical for shotcrete applications. The water-to-cement ratio was 0.5 by mass and the aggregates-to-cement ratio was 3.6. The maximum aggregate size was 10 mm. The steel fibers were of wavy shape with diameter 0.75 mm and length 25 mm. Three different volume contents were used, namely 0.5%, 1% and 1.5%. For reference purposes, a mixture of plain concrete was also produced. For each of the four mixtures three specimens were tested in bending with concurrent AE monitoring. The four-point bending experiments for the toughness determination were performed according to the ASTM C1609/C1609M-05 standard. The bottom and top spans were 300 mm and 100 mm, respectively, as shown in Fig. 1. The displacement rate was 0.08 mm/min. More details concerning the mechanical loading procedure can be found in (Soulioti and Matikas, 2008).

For the AE monitoring, two AE sensors resonant at 150 kHz (R15, Physical Acoustics Corp., PAC) were attached to the bottom side of the beams at a 50-mm distance from either side of the mid-span (see Fig. 1). The signals were amplified 40 dB and those exceeding 40 dB$_{AE}$ (in reference to 1 µV input) were recorded in a two-channel monitoring system (PCI-2, PAC). The sampling rate was 5 MHz.
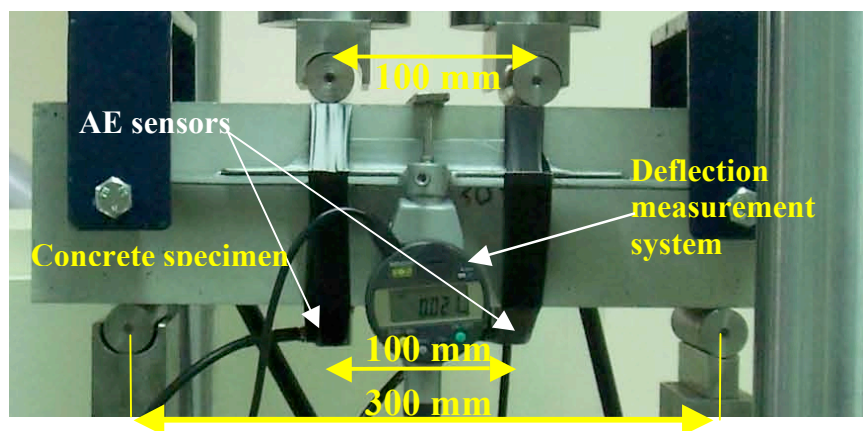


Fig. 1. Experimental setup.

**Mechanical Results**

Typical load-deflection curves of fiber-reinforced concrete specimens are depicted in Fig. 2. The behavior was typically linear up to the maximum load for all specimens. As expected, the

specimens reinforced with 1.5% of fibers exhibited higher maximum load. However, the main difference was observed in the post-peak behavior. The plain concrete failed catastrophically in two parts without absorbing any energy after the maximum load was reached. On the other hand, fiber-reinforced concrete specimens, exhibited a sudden drop of load after the initial fracture, but continued to absorb energy while their load was gradually decreased until the end of the test. As can be seen in Table 1, although the increase of fiber content did not necessarily increase the peak load of the material it certainly enhanced its flexural toughness as manifested by the area under the load-deflection curves of Fig. 2 (see also Table 1).
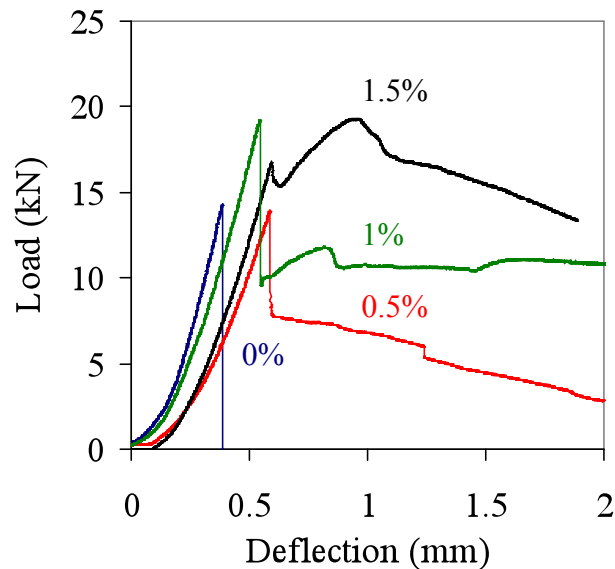


Fig. 2. Load vs. deflection curves for specimens with different fiber contents.

Table 1. Mechanical properties for different fiber contents

| Fiber Content (%) | Maximum load (kN) | Flexural toughness, $T_{100,2}$* (J) |
|---|---|---|
| 0 | 14.9 | - |
| 0.5 | 13.2 | 7.0 |
| 1 | 15.8 | 15.3 |
| 1.5 | 19.9 | 17.3 |

*The subscripts denote the specimen thickness (100 mm) and the maximum center deflection (2 mm) according to ASTM C 1609/C 1609M-05.

In Fig. 3(a), the main crack of a plain concrete specimen after failure is shown. The specimen failed in tension with the crack initiating from the bottom surface (bottom of Fig. 3(a)), which was under tensile load and propagating towards the top splitting the specimen into two parts. On the other hand, fiber-reinforced specimens did not break into two parts even after final failure. As can be seen in Fig. 3(b) the main crack was accompanied by smaller cracks. This phenomenon demonstrates the main reason for including fibers into concrete. The fracture energy is distributed in a larger volume leading to a reduction of the stress intensity. This leads to higher maximum loads of the fiber-reinforced concrete and higher absorbance of fracture energy, which was demonstrated by the increased area under the load-deflection curves of Fig. 2. As was obvious even by visual inspection the inclusion of fibers increased the width of the fracture process zone (FPZ). The same effect is also reported in the literature for large aggregates, which had a similar effect on the FPZ (Mihashi et al., 1991). As the crack propagated to the top side, it split

to different smaller cracks expanding the width of the energy absorbing zone. This bifurcation and changes of direction will be discussed along with the AE data in the next sections.
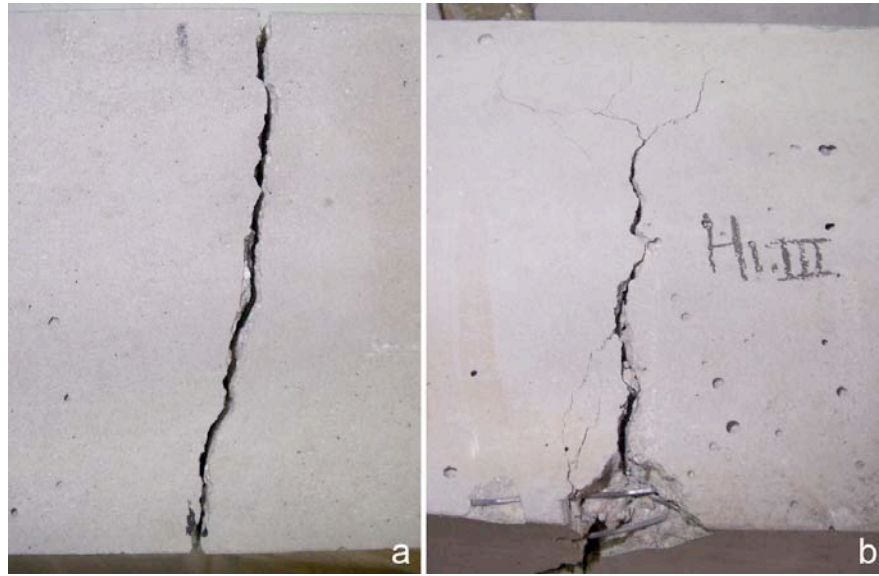


Fig. 3. (a) Cracks obtained for plain concrete, (b) concrete with 1.5% fibers.

**Acoustic Emission Results**

*Total AE hit activity*

Figures 4(a) and (b) show the history of cumulative AE hits along with the loading for typical cases of 1.5% fiber concrete and plain concrete, respectively. In the case of the specimen with fiber, at approximately 70% of the maximum load, a small increase of the AE hits was recorded and the hit rate reached a peak at the macroscopic fracture. This was demonstrated by the vertical increase of the hit line at the moment of peak load. The total number of hits was typically 3000 - 4000 (see Fig. 4(a)). However, in the case of the plain concrete specimens (Fig. 4(b)), a notably smaller number of hits were recorded. From this figure it is also obvious that immediately after the peak load the experiment was terminated due to the complete fracture of the plain specimen.

In Fig. 4(c) the total AE activity is shown for the different fiber contents. Each point is the average of the total number of hits of the three specimens of each category. The relation between the number of hits and the fiber content is close to linear. The increase of AE hits was attributed to the development of more cracks with increasing fiber content leading to a considerably larger fracture surface area. This trend of AE-hit increase corresponded to the fiber pull-out incidents, which naturally depended on the number of fibers involved in the failure zone. At the moment of the macro-crack formation (main fracture), the maximum rate of AE-hit generation was exhibited. In Fig. 4(d) the maximum hit rate (at the moment of main fracture) is shown for the different types of material. As can be seen, the fibers contributed significantly to the fracture process, even during the critical crack growth stage through the numerous pullout events (approximately 100 hits/s). On the other hand, plain concrete exhibited only 40 hits/s during the catastrophic fracture.

An interesting correlation was noticed between the number of cumulative AE hits and the toughness of the materials, as depicted in Fig. 5. As the content of fibers increased, so did the

toughness and the AE activity. As a result, with proper study, the AE activity can be used as a measure of fracture toughness.
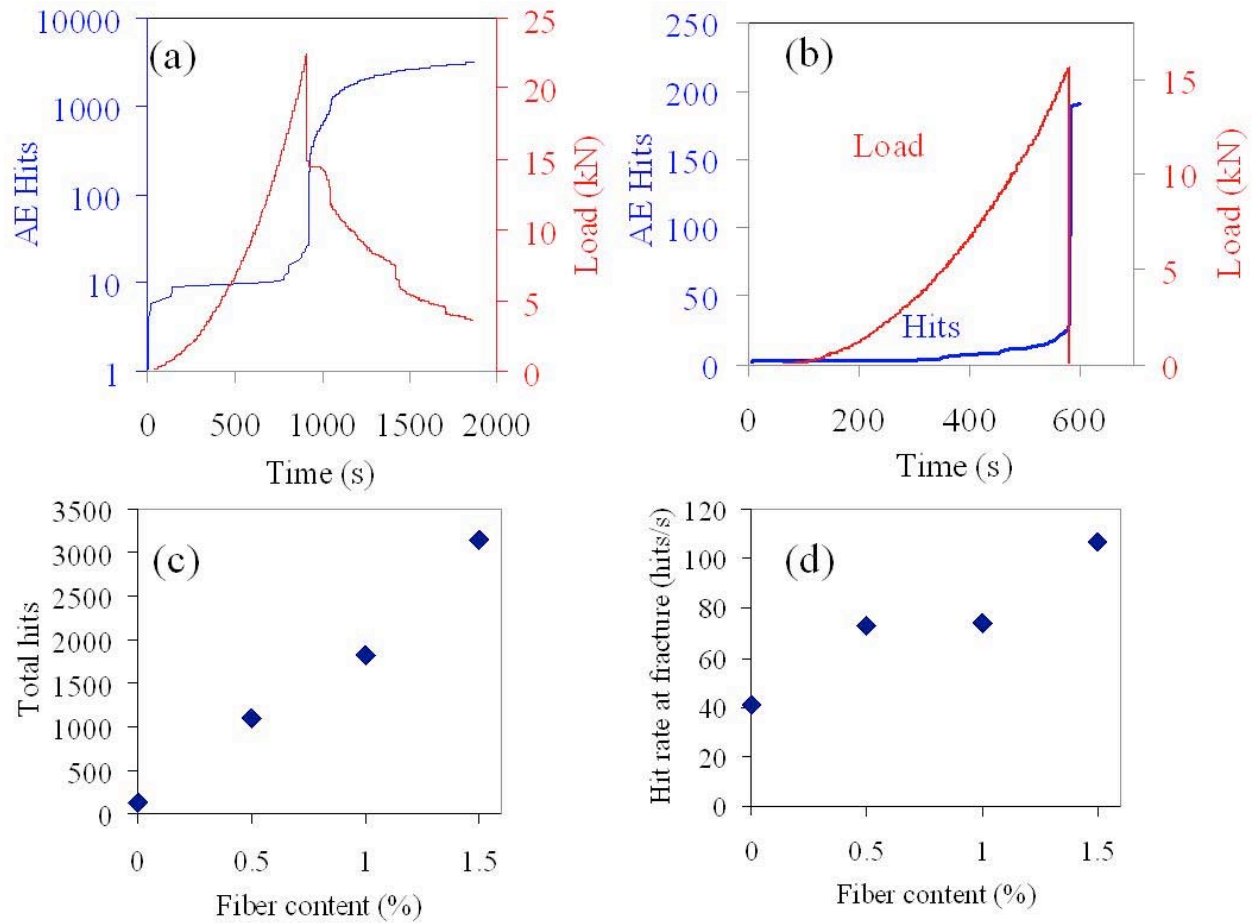


Fig. 4. Load and AE history for specimen with (a) 1.5% fibers, (b) 0% fibers, (c) total AE activity vs. fiber content, (d) maximum AE hit rate vs. fiber content.
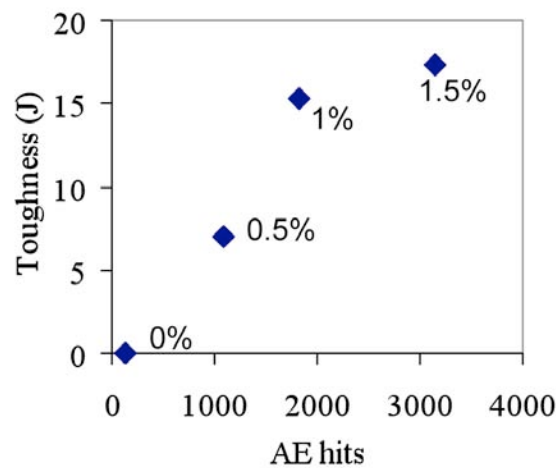


Fig. 5. Toughness vs. AE activity for different fiber contents.

*Fracture mode*

The shape of the AE waveforms is reported to be characteristic of the fracture mode. Shear events are characterized by longer rise time and higher amplitude than tensile events (Shiotani et

al., 2001). This is examined by the AE "Grade", which is defined as the ratio of waveform amplitude to the rise time. It has been shown that the higher the grade, the more tensile is the nature of the fracture events (Shiotani et al., 2001).

In the present case, the cracking process started at the bottom surface for all specimens due to the tensile stress. This implied that the initial active failure mode was tensile. In the case of the plain concrete, this failure mode was the dominant mode and led to the catastrophic failure of the specimens. However, the presence of the reinforcement changed the mode of failure of the composite. This was manifested by the creation and propagation of multiple cracks and hence a larger zone of influence together with the decrease of the grade of the AE waveforms. The grade change may be either expressed as a mean value for each fiber configuration or as a dynamic phenomenon throughout the loading process.

In Fig. 6(a), the average grade (dB/µs) is depicted for different fiber contents. As can be seen, the plain concrete specimens exhibited the highest grade from the total of the AE hits recorded throughout the experiments. The inclusion of fibers, even at just 0.5% by volume led to the considerable decrease of the grade, which was associated with the change of the failure mode from tensile to shear. Further increase of fibers had a small influence on the grade since a plateau was reached.
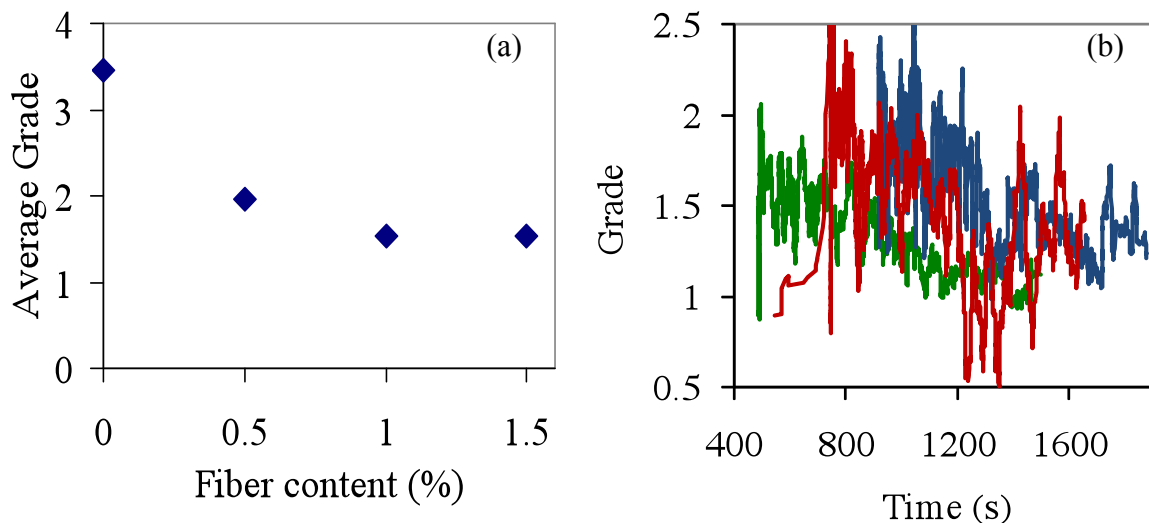


Fig. 6. (a) Average grade vs. fiber content, (b) moving average of grade for the three specimens with 1.5% fibers.

Figure 6(b) shows the change of grade vs. time for all three tests in the case of 1.5% fiber content. The curves correspond to the moving average of grade for 50 consecutive hits in order to reduce scatter. It is obvious that as the fracture proceeds, the grade gradually decreased until the end of the experiment.

Similar analysis can be conducted using the average frequency (RILEM, 2008), for which recent results showed that it drops suddenly after a strong fracture incident. This is illustrated in Fig. 7 for two specimens with 1% fibers. It is evident that at the moment the main fracture incident occurs, the average frequency of the signal drops by approximately 200 kHz (marked by arrows). Note that the symbols represent the average frequency of each hit while the black solid line stands for the moving average of the recent 40 hits. It should be highlighted that the data of Fig. 7 were captured using broadband sensors with a sensitivity range between 50 and 800 kHz

(Pico, PAC). The dynamic change of average frequency should be connected to the failure mode. Before the main fracture, matrix cracking is the most dominant mechanism. After the main fracture, fiber pull-out is added as an active fracture mechanism. The first mode resembles the mode I tensile crack while the latter resembles mode II (shear). This large frequency drop can be captured more adequately in this case than the case of resonant sensors at 150 kHz. However, the broadband sensors record only about one third of the hits a resonant sensor records in a similar experiment. Thus they are not suitable for location purposes since their sensitivity in terms of amplitude response is limited; on the other hand they prove to be more sensitive to the dynamic nature of fracture when they are located near the fracture zone.
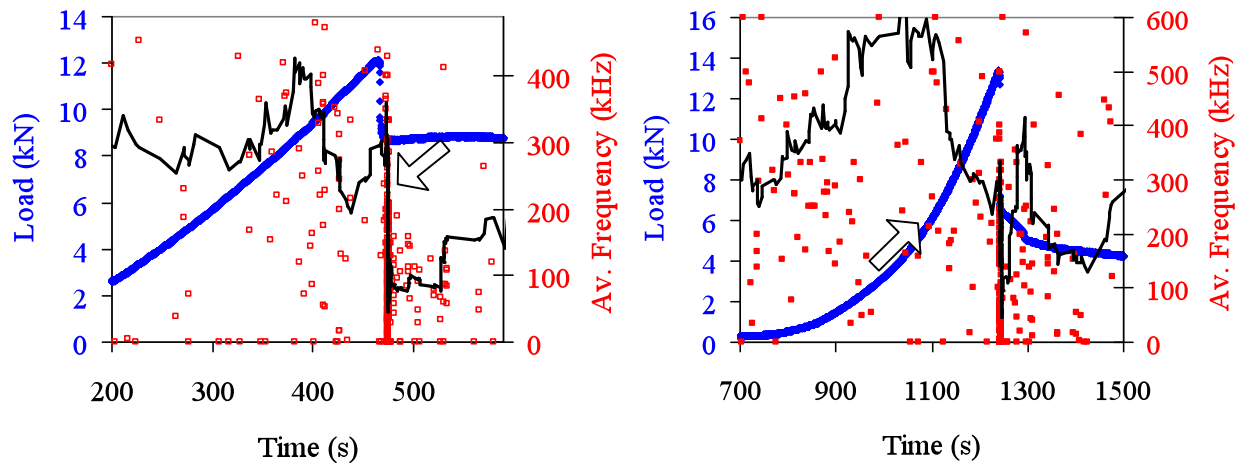


Fig. 7. Time history of load and average frequency for specimens with 1% fibers.

From the above it is shown that the nature of events is moving from tensile to shear with the propagation of damage. Although the cracks were initiated by tensile loads, gradually shear stresses dominated the failure process. This has also recently been reported for vinyl-fiber concrete (Aggelis et al. 2009). Similar behavior has been observed in corrosion cracking of concrete where crack initiation was due to the tensile mode, while as the crack length increased the shear mode became more active (Farid Uddin et al., 2004). As seen in Table 1, the increase of fiber content, which activated the shear mode was connected to the increased fracture toughness of fiber concrete. Therefore, the specimens did not break with a brittle vertical crack but the crack bifurcated to different smaller cracks on different directions, spreading the fracture energy to wider volume. It is mentioned that use of more sensors and application of inversion analysis such as Moment Tensor (Ohtsu et al., 1998) will enable the characterization of different clusters of events according to their mode type, their location in the volume of the specimen and consequently the actual width of the FPZ (Grosse and Finck, 2006).

**Conclusions**

In the present study the influence of steel fibers in concrete under bending is discussed. Macroscopically, increased fiber content resulted in the increase of the maximum load and the fracture toughness of the material. At the same time, the number of AE events was proportional to the fiber content and the measured toughness. Analysis of the "AE grade" parameter showed that the tensile mode of fracture was dominant for plain concrete, changing to shear mode as the fiber content increased. This demonstrated the definite reinforcing effect of the fibers against the weak tensile nature of concrete. As the AE activity implied, the mode of fracture changed during the experiment from tensile (initial stage) to shear (final fracture). This was macroscopically mani

fested by the crack bifurcation and deflection from parallel to perpendicular direction relatively to the loading axis and the concurrent increase of the zone of influence with increasing fiber content. The average frequency of AE hits is proved to be another parameter sensitive to the damage status especially when broadband sensors are employed.

The identification of the fracture mode, which is feasible via the acoustic emission technique, is of primary importance as it can lead to more suitable design of the reinforcement in order to withstand the specific stresses. At the same time classification of cracks can be employed for early warning prior to macroscopic failure.

The next step is the use of different types of fibers. This would reveal the best configuration in terms of volume content, fiber shape and material for the enhancement of the structural component. Furthermore, source location of the AE events via the use of more sensors can determine the actual expansion of the fracture process zone with increased fiber content.

## Acknowledgement

## References

D.G. Aggelis, T. Shiotani, S. Momoki, M. Terazawa (2007) *Advances in Acoustic Emission – 2007*, (ed. K. Ono), pp. 390-395.

D.G. Aggelis, T. Shiotani, S. Momoki, A. Hirama (2009), "Acoustic emission and ultrasound for damage characterization of concrete elements", ACI Materials Journal **106**(6). 509-514.

A.K.M. Farid Uddin, K. Numata, J. Shimasaki, M. Shigeishi, M. Ohtsu (2004), Construction and Building Materials, **18**, 181-188.

G. Fischer, V.C. Li (2007), Engineering Fracture Mechanics **74**, 258-272.

L. Golaski, G. Swit, M. Kalicka, K. Ono (2006), Journal of Acoustic Emission **24**, 187-196.

C.U. Grosse, F. Finck (2006), Cement and Concrete Composites **28**, 330-336.

B. Kim, W.J. Weiss (2003), Cement and Concrete Research **33**, 207-214.

A. Kumar, A.P. Gupta (1996), Experimental Mechanics **36**(3), 258-261.

H. Mihashi, N. Nomura, S. Niiseki (1991), Cement and Concrete Research **21**, 737-744.

B. Mobasher, H. Stang and S.P. Shah (1990), Cement and Concrete Research **20**, 665-676.

M. Ohtsu, T. Okamoto, S. Yuyama (1998), ACI Structural J. **95**(2), 87-95.

RILEM TC212-ACD (2008) Acoustic emission and related NDE techniques for crack detection and damage evaluation in concrete. Recommendation 3.

H. R. Shah, J. Weiss (2006), Materials and Structures **39**(9), 887-899.

M. Shigeishi, M. Ohtsu (1999), *Acoustic Emission: Standards and Technology Update*, ASTM STP 1353, Vahaviolos SJ, ed. American Society for Testing and Materials, pp. 175-188.

T. Shiotani, M. Ohtsu and K. Ikeda (2001), Construction and Building Materials **15**(5-6), 235-246.

T. Shiotani, D.G. Aggelis, O. Makishima (2007), Journal of Acoustic Emission **25**, 308-315.

T. Shiotani, D.G. Aggelis (2007) Journal of Acoustic Emission **25**, 69-79.

A. Sivakuram, M. Sathanam (2007), Cement and Concrete Composites **29**, 603-608.

D. Soulioti, T.E. Matikas (2008), *Proc. of the 1st Conference on Structural Materials and Components*, 21-23 May, Athens, Greece, vol. C, 1287-1298, (In Greek)

P. Stahli, J.G.M. van Mier (2007), Engineering Fracture Mechanics **74**, 223-242.

T.C. Triantafillou and C.G. Papanikolaou (2006), Materials and Structures **39**(1), 93-103.

G. Washer, P. Fuchs, B.A. Graybeal, J.L. Hartman (2004): IEEE Transactions on Ultrasonics, Ferroelectrics, and Frequency Control **51**(2), 193-201.

B. Weiler, C.U. Grosse, H.W. Reinhardt (1996), *Proceedings of the 22nd European Conference on Acoustic Emission Testing*, Aberdeen, Scotland, pp. 119-124.

K. Wu, B. Chen, W. Yao (2000), Cement and Concrete Research **30**, 1495-1500.

K. Wu, B. Chen, W. Yao (2001), Cement and Concrete Research **31**, 919-923.